

Accretion in Brown Dwarfs: an Infrared View ^{*}

A. Natta¹, L. Testi¹, J. Muzerolle², S. Randich¹, F. Comerón³, P. Persi⁴

¹ Osservatorio Astrofisico di Arcetri, INAF, Largo E.Fermi 5, I-50125 Firenze, Italy

² Steward Observatory, University of Arizona, 933 North Cherry Avenue, Tucson, AZ 85721, USA

³ European Southern Observatory, Karl-Schwarzschild-Strasse 2, 85748 Garching, Germany

⁴ Istituto Astrofisica Spaziale e Fisica Cosmica, CNR, Via del Fosso del Cavaliere, 00133 Roma, Italy

Received ...; accepted ...

Abstract. This paper presents a study of the accretion properties of 19 very low mass objects ($M_{\star} \sim 0.01 - 0.1 M_{\odot}$) in the regions Chamaeleon I and ρ Oph. For 8 objects we obtained high resolution $H\alpha$ profiles and determined mass accretion rate \dot{M}_{ac} and accretion luminosity L_{ac} . $Pa\beta$ is detected in emission in 7 of the 10 ρ Oph objects, but only in one in Cha I. Using objects for which we have both a determination of L_{ac} from $H\alpha$ and a $Pa\beta$ detection, we show that the correlation between the $Pa\beta$ luminosity and luminosity L_{ac} , found by Muzerolle et al. (1998) for T Tauri stars in Taurus, extends to objects with mass $\sim 0.03 M_{\odot}$; $L(Pa\beta)$ can be used to measure L_{ac} also in the substellar regime. The results were less conclusive for $Br\gamma$, which was detected only in 2 objects, neither of which had an $H\alpha$ estimate of \dot{M}_{ac} . Using the relation between $L(Pa\beta)$ and L_{ac} we determined the accretion rate for all the objects in our sample (including those with no $H\alpha$ spectrum), more than doubling the number of substellar objects with known \dot{M}_{ac} . When plotted as a function of the mass of the central object together with data from the literature, our results confirm the trend of lower \dot{M}_{ac} for lower M_{\star} , although with a large spread. Some of the spread is probably due to an age effect; our very young objects in ρ Oph have on average an accretion rate at least one order of magnitude higher than objects of similar mass in older regions. As a side product, we found that the width of $H\alpha$ measured at 10% peak intensity is not only a qualitative indicator of the accreting nature of very low mass objects, but can be used to obtain a quantitative, although not very accurate, estimate of \dot{M}_{ac} over a large mass range, from T Tauri stars to brown dwarfs. Finally, we found that some of our objects show evidence of mass-loss in their optical spectra.

1. Introduction

Several objects of very low mass discovered in regions of star formation have infrared excess typical of circumstellar disks (e.g., Natta and Testi 2001, Testi et al. 2002; Natta et al. 2002) and show signs of accretion-related activity (Jayawardana et al. 2002; White and Basri 2003; Muzerolle et al. 2003): they undergo an evolutionary phase similar to that of classical T Tauri stars (TTS) (Jayawardana et al. 2003b). This evidence sets potentially important constraints on the formation of very low mass objects, and on the dominance of dynamical processes in star formation in general (e.g., Bate et al. 2003), which, however, need to be made more quantitative. Statistics of disks, measurements of their masses, characterization of the accretion as a function of the mass of the central objects in regions of different age and properties are required, and are being accumulated, exploiting fully the capabilities of 8-m class telescopes.

In this paper we discuss one important parameter in this scenario, namely the accretion rate in very low mass objects, which, together with the disk mass, determines the timescale for disk survival. Mass accretion rates have been determined for a handful of very low mass objects, mostly from model-fitting of the $H\alpha$ profiles (Muzerolle et al. 2003). The results indicate that the trend of lower accretion rates for objects of lower mass, known for TTS (White and Ghez 2001; Rebull et al. 2000) continues in the substellar regime, where typical accretion rates are much lower than in TTS and can be as low as $\sim 5 \times 10^{-12} M_{\odot}/\text{yr}$ (Muzerolle et al. 2000). There is also evidence that, again as for TTS (e.g. Calvet et al. 2000), the fraction of accreting objects among very low mass objects is higher in younger regions (Jayawardana et al. 2002, 2003b). All this points to a continuity in the accretion properties across the range of mass explored so far, which suggests a similar formation mechanism from solar to sub-stellar masses.

These results, however, are based on few measurements only, and need to be confirmed. In particular, it is important to extend them to younger, more embedded regions, where the use of $H\alpha$ to derive the accretion rate is made hard or altogether impossible by the high extinction. In

Send offprint requests to: natta@arcetri.astro.it

^{*} Based on observations collected at the European Southern Observatory, Chile.

these regions, it is natural to use instead infrared hydrogen recombination lines, such as Pa β or Br γ . For TTS, it has been shown that the flux in these lines provides a good estimate of the accretion rate (Muzerolle et al. 1998). The purpose of this paper is to extend this method to the sub-stellar regime, by obtaining near-IR spectroscopy of a sample of well-known objects in two star-forming regions (Chamaeleon I and ρ Oph) for which we have also acquired and analyzed high-resolution H α profiles.

The range of masses of interest goes from the low end of the stellar range ($\lesssim 0.2 M_{\odot}$) to brown dwarfs (BD: $< 0.075 M_{\odot}$) and planetary-mass objects, below the deuterium-burning limit ($< 0.013 M_{\odot}$ or $13 M_J$). In fact, these distinctions are meaningful only “a posteriori”, when bona-fide stars reach the main sequence, not in young star-forming regions, where all objects, independently of their mass, derive their energy from contraction. For the sake of simplification (and in view of the uncertainties affecting mass determinations), we will talk in the following of very low mass objects or VLMOs.

In §2 we detail the observations, obtained with UVES and ISAAC on VLT. The results are presented in §3 and discussed in §4. A summary follows in §5.

2. Observations

2.1. Sample

We have collected a total of 19 objects, 9 in Chamaeleon I and 10 in ρ Oph. Their properties are listed in Table 1. For the Cha I sample, spectral types, effective temperatures, extinctions, luminosities and masses are from Comerón et al (2000). Quoted uncertainties are ± 150 K in T_{eff} , ± 0.2 dex in $\text{Log } L_{\star}$, and a factor of 2 in M_{\star} . Stellar parameters for the ρ Oph sources are from Natta et al. (2002), with the exception of GY10, not included in the Natta et al. sample, for which we adopt the parameters of Wilking et al. (1999). Uncertainties are ± 100 K in T_{eff} , ± 20 –30% in L_{\star} , ± 20 –40% in M_{\star} (see Testi et al. 2002 for a detailed discussion). The sample contains a number of bona-fide BDs, several objects that are either very low mass stars or relatively high-mass BDs, one object (ρ Oph-033) which has an estimated mass of $\sim 10 M_J$ only. Based on their location on the HR diagram (see Fig. 1), the VLMOs in Cha I are significantly older than those in ρ Oph (> 2 Myr versus < 1 Myr, respectively).

2.2. Low resolution near-infrared spectroscopy

Near-infrared low resolution spectra in the J and K bands were obtained for all our targets using the ISAAC near-infrared camera and spectrograph at the ESO-VLT UT1 telescope. The observations were carried out partly in Visitor Mode on April 8, 2002, and partly in Service Mode from March to July 2003 (see Table 2; Table 2 is only available in electronic form at “<http://www.edpsciences.org>”). We used the 0.6 arcsec slit and the low resolution grisms that offered a ~ 800 resolution across the wavelength

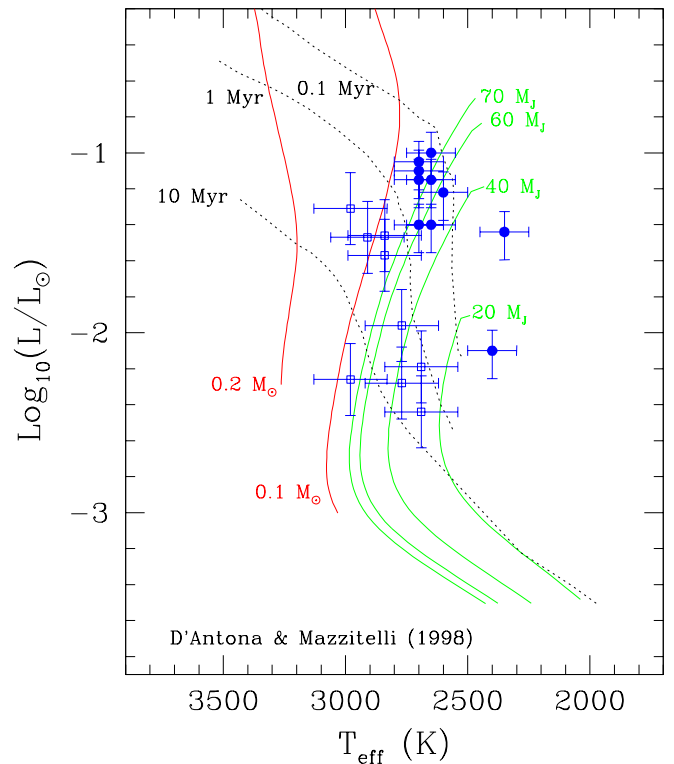


Fig. 1. Location of the sample objects in the HR diagram. Filled dots are objects in ρ Oph, open squares objects in Cha I. The tracks are from D’Antona and Mazzitelli (1997) and their unpublished 1998 update.

ranges 1.0–1.3 μm and 1.95–2.45 μm . The observing sequence was composed by a set of pairs of spectra with the target in different positions along the slit, to allow for an efficient and accurate sky subtraction. The on-source integration times varied from 25 to 40 minutes depending on target brightness and observing band (the J-band observations were typically 40–30% shorter than the K-band ones). Standard calibrations (flats and lamps) and telluric standards spectra were obtained for each observation. Wavelength calibration was performed using the lamps observations and adjusted by measuring a few OH sky lines before sky removal. We did not attempt to obtain flux calibrations.

2.3. High resolution optical spectroscopy

High resolution optical spectra for the eight brightest (in the optical bands) objects in our sample were collected using the UVES spectrograph on the ESO-VLT UT2 telescope (see Table 2). For each target a series of three to five ~ 45 min exposures were obtained in the period from March to June 2003. All spectra were obtained using the standard UVES setup with central wavelength 580nm. The chosen setup allowed us to cover a nominal spectral range from ~ 450 to 680nm. However, due to the very low signal obtained in the blue part of the spectra (450–

580 nm), only the red part was analyzed. The slit used was 12 arcsec long and 1 arcsec wide, giving a resolution $R \sim 40000$. Standard calibrations were obtained by the ESO staff as part of the Service Mode and the data were reduced using the UVES pipeline. All spectra were of excellent quality and the $H\alpha$ line was detected with high signal to noise in all individual spectra.

3. Results

3.1. Accretion rates from $H\alpha$

All eight observed objects have $H\alpha$ emission, in seven cases with equivalent width $\gtrsim 10$ Å. Of these, five (2 in Cha I and 3 in ρ Oph) show in all our observations broad $H\alpha$ profiles. This, as discussed by White and Basri (2003) and Jayawardana et al. (2002), is indication of accretion-related rather than chromospheric activity. For each of these objects, we have computed an average profile, shown in Fig. 2, and compared it to the prediction of the magnetospheric accretion models developed by Muzerolle et al. (2001) and recently applied to a sample of sub-stellar objects by Muzerolle et al. (2003). Accretion rates derived from $H\alpha$ profiles agree well with those obtained from veiling in TTS (e.g., Muzerolle et al. 1998) and in the few VLMOs for which \dot{M}_{ac} could be estimated from veiling measurements (Muzerolle et al. 2003).

The underlying assumption is that the entire $H\alpha$ (as well as the other hydrogen lines) comes from accreting matter, and that the contamination from wind/jet emission is negligible. This is not necessarily true in all strongly accreting TTS (see, for example, Bacciotti et al. 2002), but is probably a good approximation for our objects (see §3.4).

For all objects we have adopted a stellar mass $M_* = 50 M_J$, radius $0.5 R_\odot$ and a magnetospheric truncation radius of $2.2\text{--}3 R_*$. The results are not very sensitive to the exact values of these parameters. The fitting procedure gives for each object a value of \dot{M}_{ac} and of the inclination angle i . The resulting accretion rates are given in Table 1; they range from $10^{-9} M_\odot/\text{yr}$ for ρ Oph-102 to $\sim 10^{-11} M_\odot/\text{yr}$ for ρ Oph-030. The inclination angle is $\sim 65\text{--}75$ deg for Cha H α 2, ρ Oph-030, ρ Oph-032, ~ 80 deg for Cha H α 6, and ~ 30 deg for ρ Oph-102. The fits are of acceptable quality, with the exception of Cha H α 2, whose broad and flat profile (clearly present in all the observations) cannot be reproduced by the current models (similar profiles are observed in few other VLMOs and discussed in Muzerolle et al. 2003). The fit can be somewhat improved by adopting an ad-hoc temperature profile for the accretion flow, whereby the temperature has been reduced relative to the fiducial model in the outer part of the flow near the disk. This results in less emission near the line center, the most uncertain part of the profiles given the approximations used in the radiative transfer calculations (see Muzerolle et al. 2001). Nevertheless, both models for Cha H α 2 have similar inclination and an accretion rate of the order of $10^{-10} M_\odot/\text{yr}$, which we will adopt in the following. As

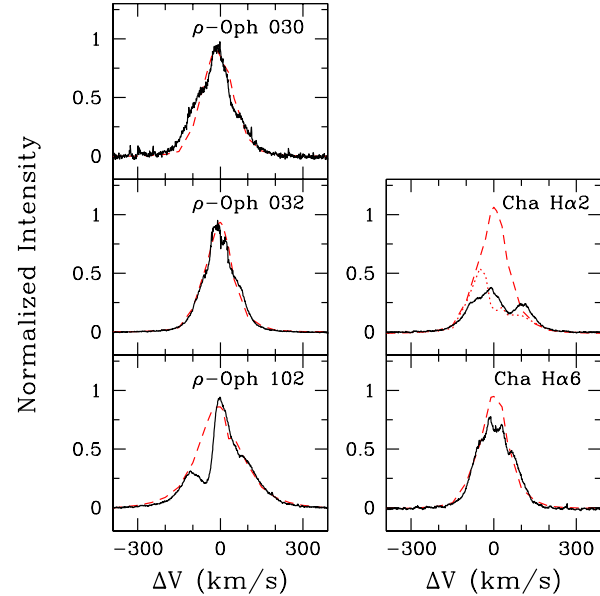


Fig. 2. Normalized average $H\alpha$ profiles for the 5 objects with broad lines. The solid curves are the observed profiles, the dashed ones are the model fits. For Cha H α 2, the dotted lines shows a model with an ad-hoc temperature profiles (see text). The stellar continuum has been subtracted.

discussed by Muzerolle et al. (2003), the values of \dot{M}_{ac} derived from the $H\alpha$ profiles should be accurate within a factor of $\sim 3\text{--}5$.

A second group of 3 objects, all in Cha I, (Cha H α 1, Cha H α 3, Cha H α 5) has always narrow $H\alpha$ profiles, typical of chromospheric activity. For these objects, we estimate an upper limit to \dot{M}_{ac} of about $10^{-12} M_\odot/\text{yr}$, for which the magnetospheric accretion models predict a line emission below the detection limit.

In Fig. 3 we compare our estimates of \dot{M}_{ac} to those of other VLMOs and TTS from the literature. The figure plots \dot{M}_{ac} as a function of the full width of $H\alpha$ measured at 10% of the peak intensity (after continuum subtraction). Dots are VLMOs (mass $\lesssim 0.2 M_\odot$), where \dot{M}_{ac} is measured by fitting the $H\alpha$ profiles (filled dots from this paper, open dots from Muzerolle et al. 2003); pentagons are VLMOs with values of \dot{M}_{ac} high enough to produce measurable veiling in the optical (White and Basri 2003; Muzerolle et al. 2000, 2003; Barrado y Navascués et al. 2004). The squares show the location on this diagram of a sample of more massive TTS, from which \dot{M}_{ac} has been derived from veiling (Gullbring et al. 1998), and the 10% $H\alpha$ width are from high resolution $H\alpha$ profiles obtained by Edwards et al. (1994). The total sample spans a range of masses from about 0.04 to $0.8 M_\odot$. Fig. 3 shows that our determinations of \dot{M}_{ac} agree with the general trend shown by other objects from the literature, and that there is conti-

Table 1. Object Properties and Hydrogen Lines

Star	ST	T _{eff} (K)	LogL _★ (L _☉)	A _V (mag)	M _★ (M _J)	Hα10% (km/s)	EW(Hα) ^a (Å)	EW(Paβ) ^a (Å)	EW(Brγ) ^a (Å)	Log \dot{M}_{ac}^b (M _☉ /y)	Log \dot{M}_{ac}^c (M _☉ /y)
Cha Hα1	M7.5	2770	-1.96	0.2	40	155	35	<0.3	<1	< -12	< -11.4
Cha Hα2	M6.5	2910	-1.47	0.8	70	366	33	0.3	<1.5	-10.0	-10.8
Cha Hα3	M7	2840	-1.46	0.3	60	142	10	<0.9	<1.2	< -12	< -10.1
Cha Hα5	M6	2980	-1.31	1.0	100	137	6.5	<0.9	<1.7	< -12	< -10.0
Cha Hα6	M7	2840	-1.57	0.26	50	274	48	<0.3	<1	-10.5	< -10.8
Cha Hα7	M8	2690	-2.19	0.3	30	–	–	<0.6	<1.0	–	< -11.1
Cha Hα9	M6	2980	-2.26	1.5	70	–	–	<0.6	<1.0	–	< -11.4
Cha Hα10	M7.5	2770	-2.28	0.1	40	–	–	<0.3	<0.9	–	< -12.0
Cha Hα11	M8	2690	-2.44	0.0	30	–	–	<0.3	<0.9	–	< -12.1
ρ Oph-023	M7	2650	-1.40	8.0	40	–	–	1.80	<1	–	-9.3
ρ Oph-030	M6	2700	-1.15	3.0	60	292	30	0.30	<1	-10.8	-10.1
ρ Oph-032	M7.5	2600	-1.22	2.0	40	248	50	0.40	<0.9	-10.5	-9.8
ρ Oph-033	M8.5	2400	-2.10	7.0	10	–	–	<0.7	<2.1	–	< -10.3
ρ Oph-102	M6	2700	-1.10	3.0	60	377	40	2.0	<1	-9.0	-8.9
ρ Oph-160	M6	2700	-1.40	6.0	45	–	–	3.3	4.0	–	-9.0
ρ Oph-164	M6	2700	-1.05	6.0	60	–	–	0.80	<1.6	–	-9.3
ρ Oph-176	M6	2650	-1.15	7.0	50	–	–	<0.5	<1.3	–	< -9.7
ρ Oph-193	M6	2650	-1.00	7.5	60	–	–	1.8	2.9	–	-8.9
ρ Oph-GY10	M8.5	2350	-1.44	18	30	–	–	<0.5	<1.0	–	< -9.0

^a Positive values indicate emission.

^b Accretion rates from Hα profiles.

^c Accretion rates from Paβ luminosities.

nity between measurements obtained from veiling (which are fully independent of the Hα width) and those derived from Hα profiles.

In the sub-stellar regime, the Hα10% width, which can be derived directly from the observations, is considered a good indicator of accretion, with the separation between accretors and non-accretors set at Hα10% width between ~ 200 km/s (Jayawardana et al. 2003b) and ~ 270 km/s (White and Basri 2003). Fig. 3 confirms this result. Adopting ~ 200 km/s as a limit, one would missclassify one accreting object out of 23 (MHO-4, with $\dot{M}_{ac} \sim 1.5 \times 10^{-11}$ M_☉/yr and Hα 10% width of 154 km/s; Muzerolle et al. 2003) and two non accretors (V927 Tau and USco CTI-O75) out of the 37 for which there are \dot{M}_{ac} upper limits (Muzerolle et al. 2003 and this paper). Furthermore, Fig. 3 shows that there is a rather good correlation between the Hα 10% width and \dot{M}_{ac} over the whole range of mass from BDs to TTS, so that it is possible to use the observed width not only to discriminate between accretors and non-accretors but also to get an approximate estimate of the accretion rate, without performing detailed model fits. We show in Fig. 3 the best-fit relation between these two quantities for Hα 10% width > 200 km/s, which can be expressed as:

$$\text{Log}\dot{M}_{ac} = -12.89(\pm 0.3) + 9.7(\pm 0.7) \times 10^{-3} \text{H}\alpha 10\% \quad (1)$$

where Hα10% is the Hα 10% width in km/s and \dot{M}_{ac} is in M_☉/yr.

The spread is rather large, and can be due in part to the fact that in most cases the measurements used to derive \dot{M}_{ac} and the high-resolution Hα profiles have not been obtained simultaneously. We show, as an illustration of possible problems, the rather unusual case of the TTS DF Tau which has an accretion rate of about 10^{-7} M_☉/yr, based on veiling from medium-resolution spectrophotometric data obtained in 1996 (Gullbring et al. 1998). High resolution profiles of several Balmer lines obtained non-simultaneously from 1988 to 1990 by Edwards et al. (1994), show broad emission in all the lines, but with large discrepancies between them; in particular, the Hα width is smaller than that of the higher Balmer lines. One could certainly improve the correlation if larger and simultaneous sets of data for TTS were available. \dot{M}_{ac} values derived in this way are necessarily inaccurate for individual objects, and should be used with care. Nevertheless, they can be very useful when dealing with large samples of objects.

3.2. Paβ and Brγ as accretion indicators

Our near-IR spectroscopy does not allow us to resolve the line profiles, and we can only measure equivalent widths, listed in Table 1. Of the 9 Chamaeleon I objects, Paβ

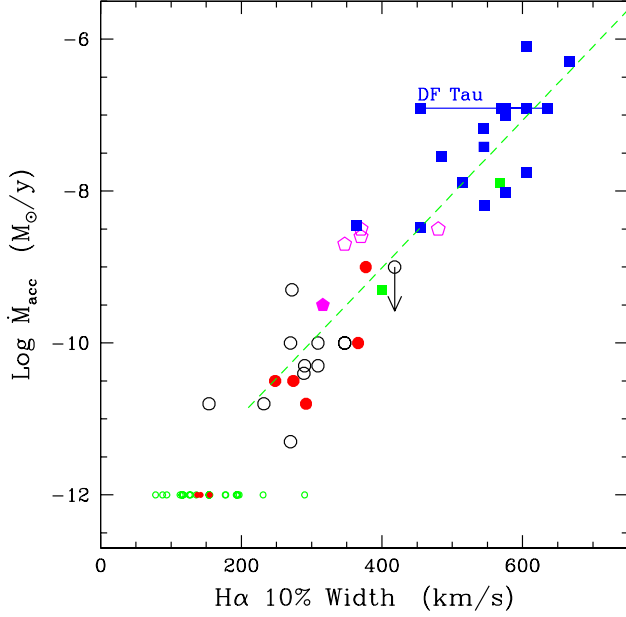


Fig. 3. Accretion rate as a function of the H α full width at 10% peak intensity. Dots (full and open) and pentagons are objects with mass $\lesssim 0.23 M_{\odot}$. Full dots are from this paper, open dots from Muzerolle et al. (2003); for both samples \dot{M}_{ac} has been derived from model-fits of the H α profiles. Pentagons are substellar objects for which \dot{M}_{ac} has been obtained from veiling measurements (Muzerolle et al. 2003, 2000, White and Basri 2003; Barrado y Navascués et al. 2004). The small dots at $\text{Log } \dot{M}_{ac} = -12$ are VLMOs with no evidence of accretion (37 in total); the value of the accretion rate is the model-determined upper limit. Squares are TTS (mass $\gtrsim 0.3 M_{\odot}$) for which accretion rates have been measured from veiling. Most are TTS in Taurus-Auriga (\dot{M}_{ac} from Gullbring et al. 1998, H α widths from Edwards et al. 1994). We have also added TW Hya (Muzerolle et al. 2000) and GN Tau from White and Basri (2003). The dashed line shows the best-fitting relation (Eq. 1). The four connected squares show the 10% full width of H α , H β , H γ and H δ for DF Tau from Edwards et al. (1994); H α is the narrowest of the four.

is detected in only 1. For the others, we can set upper limits to the equivalent width (3σ) of about 0.3–0.9 Å. In Ophiucus, on the contrary, we detect Pa β emission in 7 of the 10 observed objects. Br γ is detected only in 2 objects in ρ Oph. Of the 5 objects with evidence of accretion from H α , Pa β is detected in 4, while Br γ is not detected in any. Fig. 4 shows the spectra of the objects with line detections.

These results suggest that Br γ , which is intrinsically weaker than Pa β , is more difficult to detect even in highly reddened objects, where differential extinction favors lines at longer wavelengths. For this reason, we will focus in the following on the use of Pa β as an accretion indicator. We have therefore converted equivalent widths into

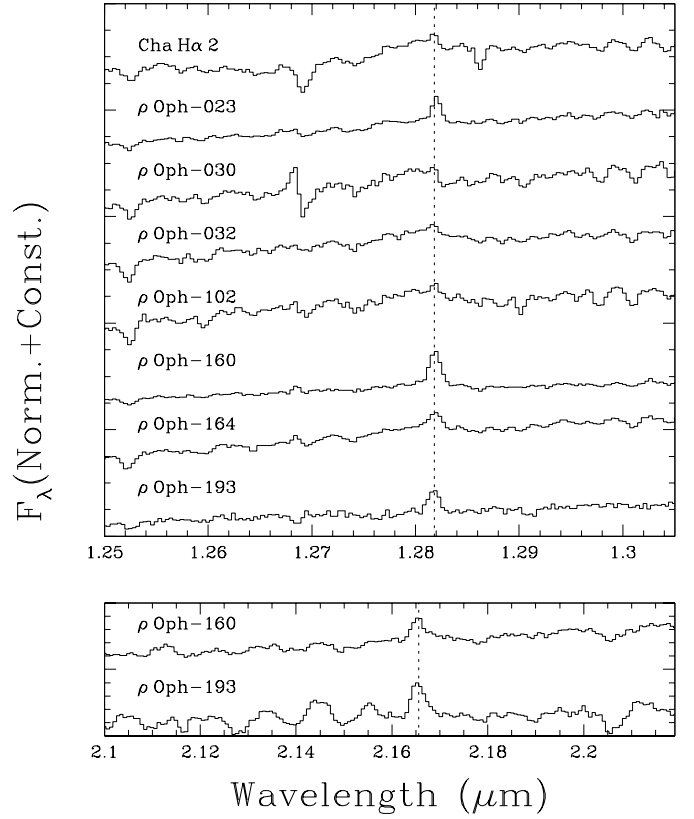


Fig. 4. Near-IR spectra of objects with Pa β (top panel) or Br γ (bottom panel) detection.

fluxes using broad-band magnitudes and then correcting for extinction for the Cha I objects, while for the ρ Oph objects we have used the calibrated low-resolution spectra of Natta et al. (2002) for the continuum and corrected for extinction the resulting line fluxes.

Fig. 5 shows the relation between the Pa β luminosity (derived from the measured fluxes assuming a distance of 150 pc for Ophiucus and 160 pc for Cha I) and the accretion luminosity, computed from \dot{M}_{ac} and the stellar parameters given in Table 1. According to Muzerolle et al. (1998), these two quantities (rather than line flux versus \dot{M}_{ac}) show the tightest correlation in TTS, and we have added Muzerolle’s sample to ours. The figure shows that the trend of lower Pa β luminosity for lower L_{ac} extends to the very low values of L_{ac} which characterize VLMOs. In fact, one can derive a rather good relation to estimate L_{ac} from the Pa β luminosity over the whole range of masses from few tens of Jupiter masses to about one solar mass, shown by the dashed line in Fig. 5 and given by:

$$\text{Log } L_{ac} = 1.36(\pm 0.2) \times \text{Log } L(\text{Pa}_{\beta}) + 4.00(\pm 0.2) \quad (2)$$

where L_{ac} and $L(\text{Pa}_{\beta})$ are in units of L_{\odot} . Note that this relation is, within the uncertainties, identical to that derived by Muzerolle et al. (1998) for TTS over a much narrower interval of $L(\text{Pa}_{\beta})$.

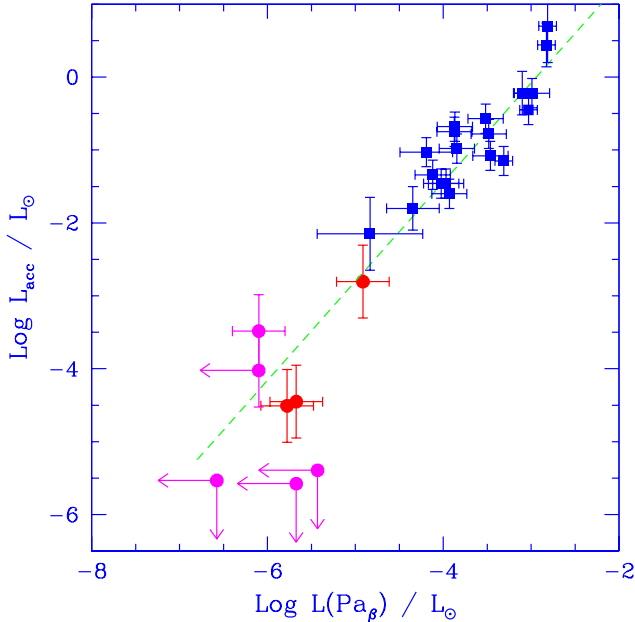


Fig. 5. $\text{Pa}\beta$ luminosity as a function of L_{ac} . The dots are the VLMOs from this paper. The squares are T Tauri stars in Taurus-Auriga from Muzerolle et al. (1998). The dashed line is the best-fitting relation (Eq. 2).

As for $\text{H}\alpha$ we have ignored the possibility that some $\text{Pa}\beta$ emission may come from wind or jets, driven by accretion. In several TTS, the profiles of $\text{Pa}\beta$ and $\text{Br}\gamma$ are well described by magnetospheric accretion models (Folha and Emerson 2001), but there are some examples of $\text{Pa}\beta$ wind emission (Whelan et al. 2004). Inspection of Fig. 5 shows that, very likely, any correction for a wind/jet contribution to the $\text{Pa}\beta$ luminosity will be lost within the uncertainties of the individual measurements and the large scatter of the points. Nevertheless, the possibility of a contribution from outflowing matter to lines should be kept in mind when discussing individual objects.

Using the relation (2), we have derived L_{ac} and \dot{M}_{ac} for all the objects in our sample; \dot{M}_{ac} is given in the last column of Table 1. The largest differences between this determination of \dot{M}_{ac} and that from the $\text{H}\alpha$ profile is of the order ± 0.7 – 0.8 in log, i.e., a factor ~ 6 (see also Fig. 5).

3.3. Variability

Spectroscopic and photometric variability over a large interval of timescales is typical of pre-main sequence stars of all mass, including sub-stellar objects. By necessity, this introduces an artificial spread in correlation such as those of Fig. 3 and 5, when the accretion rate or luminosity and the line properties are not measured simultaneously. We expect that the quality of these correlations could improve significantly if simultaneous observations were available.

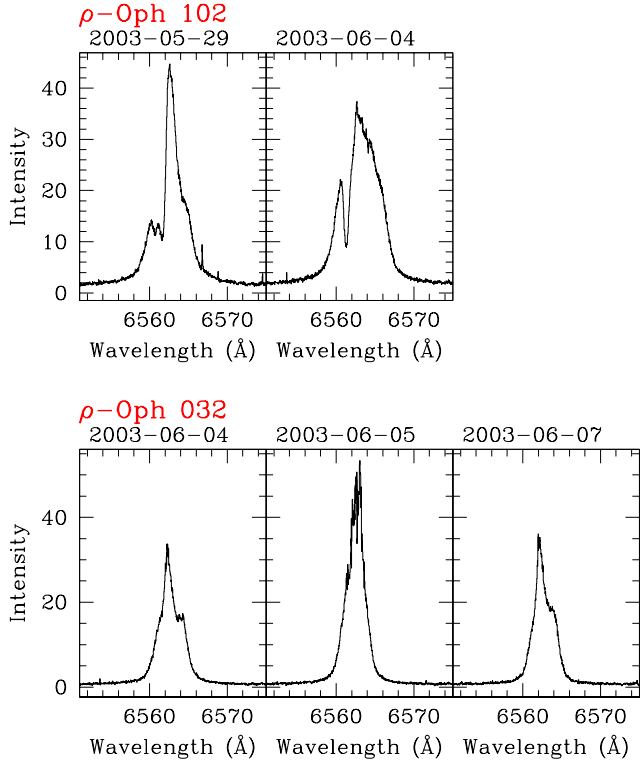


Fig. 6. $\text{H}\alpha$ variability in ρ Oph-102 and ρ Oph-032.

Another consequence of variability is the difficulty of assigning a well-defined accretion rate to any specific star. Variations of the $\text{Br}\gamma$ flux are typically within a factor 2–3 (see, for example, Greene and Lada 1997; Luhman and Rieke 1998); if similar variations apply to $\text{Pa}\beta$ (for which we could not find multiple-epoch data in the literature) this would change the estimate of L_{ac} by a factor ~ 2 – 5 . In some cases, the lines become undetectable, and one would then classify the star among non-accretors.

Similar uncertainties are obtained if we consider the variations of the $\text{H}\alpha$ 10% width. In our spectra (see Fig. 6), the largest variation is seen in ρ Oph-102, where the $\text{H}\alpha$ 10% width varies from 335 km/s on May 29, 2003 to 411 km/s on June 4, 2003. According to eq.(1), the corresponding accretion rate would increase by a factor ~ 5 . In all the other objects the $\text{H}\alpha$ variations are smaller, implying a maximum change of \dot{M}_{ac} of a factor ~ 3 at most. A comparison of the sub-stellar objects in IC 348 for which $\text{H}\alpha$ profiles have been obtained by Muzerolle et al. (2003) and Jayawardana et al. (2003b) shows variations that would result in changes of L_{ac} again by a factor ~ 2 – 5 , according to Eq.(1).

An interesting case is that of ρ Oph-030 (GY 5), which has a strong $\text{H}\alpha$ emission in our and Jayawardana et al. (2002) spectra (but a very different profile and a 10% $\text{H}\alpha$ width of 292 and 352 km/s respectively) but is narrow (177 km/s) and weak in the spectrum of Muzerolle et al. (2003).

Some of these variations may be due to differences in the quality of the spectra (resolution, signal-to-noise etc.),

since all the VLMOs are very weak, often close to the instrumental limits. Still, most of the variability is likely to be real, as suggested by very similar results in TTS. For any individual object, one should have high quality spectra and long time sequences, which could provide not an instantaneous but a “typical” accretion rate. However, if we consider a large sample of objects, these individual variations will average up and will only increase the spread of any existing correlation, but not change it systematically.

3.4. Other Optical Lines

The UVES spectral range contains a number of other emission lines (in addition to $H\alpha$), usually considered good indicators of mass-loss and accretion. Table 3 gives the equivalent width of the lines (positive values for emission) and, in some cases, as for the NaD doublet, some information on their profile. The spectrum of Cha H α 1 is too noisy, and we have dropped this object from the table.

The HeI lines are generally interpreted as emitted in the accretion shock at the base of the infalling matter: these lines are indeed present and measurable in all the objects where we detect accretion in $H\alpha$ (Cha H α 2, Cha H α 6, ρ Oph-030, ρ Oph-032 and ρ Oph-102), but not in Cha H α 3 and 5, which have narrow $H\alpha$ profiles and no evidence of accretion. This result is consistent with our $H\alpha$ analysis.

Some of the objects show indications of outflows. These are particularly strong in ρ Oph-102, which has emission in all the forbidden lines of [OI], [NII], [SII], and shows a P-Cygni profile in the NaD doublet (see Fig. 7), but also ρ Oph-32, Cha H α 2 and Cha H α 3 have detectable emission in some of the forbidden lines, and clear emission in the NaD doublet. All these objects are good candidates for further studies of winds and jets in VLMOs. However, there is no evidence of H_2 vibrationally excited emission in the IR spectra of our objects, with the possible exception of ρ Oph-033, where, however, it is likely due to contamination from VLA 1623 (see also Williams et al. 1995).

Weak accretion-driven winds are expected in VLMOs, if they behave as TTS. Note, however, that even in ρ Oph-102 the equivalent width of $H\alpha$ is much larger than that of the [SII] lines (the ratio is ~ 200). The weakness of the forbidden lines in comparison to $H\alpha$ in our objects supports the assumption that the hydrogen lines form mostly in the accreting gas (see also Fernández and Comerón 2001 and references therein).

As well known the presence of Li is a strong indication of substellar nature and/or youth. The covered spectral range includes the Li I doublet at 6708 Å. We detect it in absorption in all but one objects with equivalent widths ranging between 0.2 and 0.5 Å, confirming, in combination with the late-M spectral types, that they are members of the clouds. The Li line is not detected in Cha H α 1; we believe this is due to the very low S/N of the spectrum

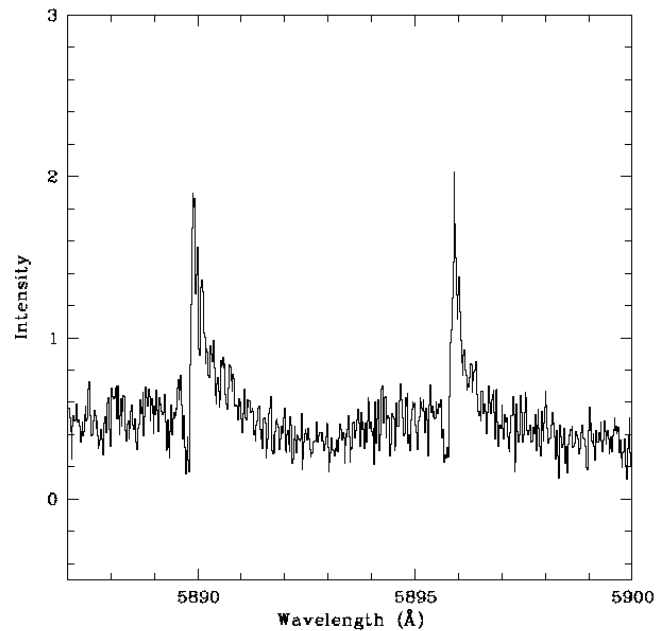


Fig. 7. NaD lines in ρ Oph-102.

which shows virtually no continuum (see also Jörgens and Günther 2001).

4. Discussion

4.1. Accretion as a function of mass and age

Our sample of VLMOs more than double the number of objects with measured \dot{M}_{ac} . We plot in Fig. 8 our results, together with a compilation of data from the literature, as a function of the mass of the central object. The data include TTS and VLMOs, spanning a range of masses of about two orders of magnitude. All the masses have been redetermined self-consistently using the same evolutionary tracks (1998 unpublished update of D’Antona and Mazzitelli 1997), and the accretion rates have been scaled to these values, when necessary. Note that we have plotted upper limits for \dot{M}_{ac} only for objects from this paper.

Both \dot{M}_{ac} and M_\star have large uncertainties, discussed in detail, among others, by Muzerolle et al. (2003) and in this paper. There are, however, some clear trends. First of all, Fig. 8 confirms, over a large range of masses, the trend already found by other authors (Muzerolle et al. 2003; Rebull et al. 2000) of decreasing \dot{M}_{ac} for decreasing M_\star . If, for example, we compare the median \dot{M}_{ac} for $M_\star < 0.1 M_\odot$ to that in the mass interval 1–0.3 M_\odot , we find values of $\sim 3 \times 10^{-10}$ and $\sim 10^{-8} M_\odot/\text{yr}$, respectively (neglecting upper limits to \dot{M}_{ac}). It is unlikely that this trend is caused by sensitivity limits. Although, as we will discuss in the following section, in many VLMOs the accretion rate is close to the model sensitivity, this is not the case of TTS (see, e.g., Muzerolle et al. 2003), so that the correlation we find neglecting upper limits is probably somewhat shallower than the true one.

Table 3. Equivalent width of other optical emission lines

Object	[OI] λ 6300 (\AA)	[OI] λ 6363 (\AA)	[NII] λ 6583 (\AA)	[SII] λ 6716 (\AA)	[SII] λ 6731 (\AA)	HeI λ 5875 (\AA)	HeI λ 6678 (\AA)	NaI λ 5896,5890 ^a
Cha H α 2	–	–	0.06:	0.06:	<0.1	1.6	0.6	E(PCyg)
Cha H α 3	–	–	0.03:	< 0.1	0.08	< 0.1	< 0.1	E
Cha H α 5	–	–	< 0.1	< 0.08	< 0.1	< 0.2	< 0.08	E
Cha H α 6	–	–	0.07	< 0.08	< 0.08	1.1	0.3	E
ρ Oph-030	–	–	< 0.1	< 0.08	< 0.08	1.0	0.3:	E
ρ Oph-032	–	–	0.1:	0.12:	< 0.1	6.0	2.2	E
ρ Oph-102	2:	0.4:	0.1:	0.07	0.2:	4.4	2.3	E(PCyg)

^a E: both components in emission; PCyg: additional blue-shifted absorption (see Fig. 7).

A second effect is clearly shown in Fig. 8, namely that the accretion rate, for the same mass of the central object, is higher in younger regions. The ρ Oph brown dwarfs have accretion rates of roughly 10^{-9} – 10^{-10} M_{\odot}/yr , more than an order of magnitude larger than most objects of similar mass in Taurus, Chamaeleon and IC 348. An age dependence of \dot{M}_{ac} is known in TTS (e.g., Calvet et al. 2000), and is suggested for VLMOs by the fact that the fraction of objects with narrow H α profiles (non-accretors) is larger in older star forming regions (Jayawardana et al. 2002, 2003b). Our results confirm this trend: only 10% (1 out of 10) of the objects in our Cha I sample are accreting; if we include also the Gómez and Persi (2001) VLMOs, then the fraction becomes 28% (5 out of 18 objects).

The dependence of \dot{M}_{ac} on age makes it hard to determine the exact relationship of \dot{M}_{ac} vs. M_{\star} from samples where objects in regions of very different age are collected together, as in Fig. 8. For example, the ρ Oph BD population selected by Natta et al. (2002) is particularly young, and it would be interesting to compare their accretion rates to equally young TTS in ρ Oph, rather than to TTS in Taurus. Also, there are a few VLMOs in Taurus, Cha I and IC348 with very large accretion rates, comparable or even higher than those of the ρ Oph VLMOs. Some of these estimates need to be confirmed, and the possibility of having detected a flare ruled out. Still, one wonders if they could be much younger than the average population of the star-forming region to which they belong.

In spite of the large uncertainties that affect individual objects, these preliminary results show that it is now possible, with the advent of 8-m class telescopes that give access to the VLMOs population, to quantify the dependence of \dot{M}_{ac} on mass and age, overcoming, due to the large range of M_{\star} that one can explore, the uncertainties of individual measurements. For this one needs larger and more homogeneous samples of stars (not only VLMOs but also TTS) in a variety of star-forming regions.

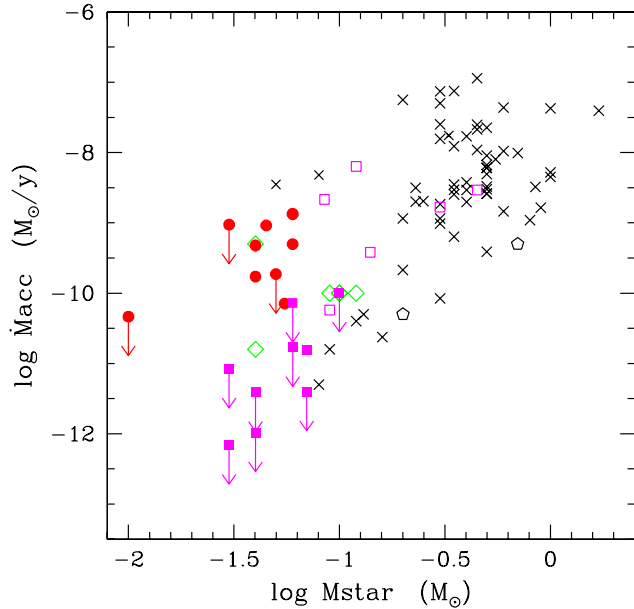


Fig. 8. Accretion rate as a function of the mass of the central object. Filled dots and squares are VLMOs in ρ Oph and Cha I, respectively, from this paper; \dot{M}_{ac} has been determined from L(Pa β) as described in §3.3. Arrows are 3σ upper limits. Open squares are objects in Cha I from Gómez and Persi (2001) with Pa β emission, where \dot{M}_{ac} has been determined from L(Pa β). Objects in IC 348 (Muzerolle et al. 2003) are shown by diamonds, in TW Hya (Muzerolle et al. 2000) by pentagons, in Taurus (White and Ghez 2001, White and Basri 2003, Muzerolle et al. 2003) by crosses. We do not plot objects from the literature with no detected accretion.

4.2. Disks and Accretion

Classical TTS show a clear correlation between accretion and the presence of a circumstellar disk. Disks are detected around a number of VLMOs, which show mid-

Table 4. Correlation between accretion and mid-IR excess

Star	Acc. (H α)	Acc. (Pa β)	Acc. (Br γ)	6.7 μ m	14.3 μ m
Cha H α 1	N	N	N	Y	Y
Cha H α 2	Y	Y	N	Y	Y
Cha H α 3	N	N	N	Y	N
Cha H α 5	N	N	N	Y	N
Cha H α 6	Y	N	N	Y	N
Cha H α 7	–	N	N	N	N
Cha H α 9	–	N	N	Y	Y
Cha H α 10	–	N	N	N	N
Cha H α 11	–	N	N	N	N
ρ Oph-023	–	Y	N	Y	Y
ρ Oph-030	Y	Y	N	Y	Y
ρ Oph-032	Y	Y	N	Y	Y
ρ Oph-033	–	N	N	Y	Y
ρ Oph-102	Y	Y	N	Y	Y
ρ Oph-160	–	Y	Y	Y	Y
ρ Oph-164	–	Y	N	Y	Y
ρ Oph-176	–	N	N	Y	Y
ρ Oph-193	–	Y	Y	Y	Y
ρ Oph-GY10	–	N	N	Y	Y

infrared fluxes well in excess of the photospheric ones (e.g., Comerón et al. 1998, Persi et al. 2000, Bontemps et al. 2001), modeled as the emission of disks heated by radiation from the central objects (Natta and Testi 2001, Testi et al. 2002; Natta et al. 2002).

Table 4 summarizes the information on the presence of a mid-IR excess in our sample objects. All 10 objects in ρ Oph have been detected by ISOCAM at 6.7 and 14.3 μ m (Bontemps et al. 2001), and the correlation between disk and accretion, i.e., broad H α and/or emission in the hydrogen IR lines, is basically confirmed by the results of this paper.

The Chamaeleon sample is in a way more intriguing. Three objects (Cha H α 1, Cha H α 2, Cha H α 9) have excess emission at 6.7 and 14.3 μ m (Persi et al. 2000), modeled by Natta and Testi (2001) as due to disks. Of these, Cha H α 2 is clearly accreting, Cha H α 1 and Cha H α 9 (for which we have no H α profile) do not. Three objects have been detected at 6.7 μ m, but not at 14.3 μ m; of these, Cha H α 3 and Cha H α 5 do not show evidence of accretion in H α nor in Pa β or Br γ , while Cha H α 6 has broad H α , but no emission in the IR lines. Finally, three (H α 7, H α 10 and H α 11) have no detected mid-IR excess and no IR line emission.

It appears from these results that disks are detected more easily than accretion, and that there is a population of VLMOs with evidence of disks but no detectable accretion activity. This is somewhat different from TTS, where most WTTS have no evidence of accretion but also

no detectable IR excess (as some of the Cha I objects). This is probably due to the fact that even in very active VLMOs the accretion rate is close to the sensitivity limit of the various methods one can use, making it difficult to discriminate between “accretors” and “non-accretors”. On the contrary, in TTS typical accretion rates are at least two orders of magnitude higher than the sensitivity limit of veiling measurements and/or H α profile fitting (Gullbring et al. 1998; Muzerolle et al. 2003), and the separation between accreting and non-accreting objects is therefore much more meaningful.

One of the implications of the very low accretion rates that characterize BDs is that their disks should live long. If we assume, for example, that the disk mass scales with the mass of the central objects in BDs as in TTS, we have typical disk masses of about $10^{-3} M_{\odot}$; with an accretion rate of $\sim 3 \times 10^{-10} M_{\odot}/\text{yr}$, as measured in ρ Oph, the disk will live at least 3×10^6 years, as a typical TTS. This agrees with the results of Liu et al. (2003), who found no significant difference in the fraction of disks between BDs and TTS, and that the age of the TTS with disks was similar to that of TTS without disks.

It is more difficult to use this same result to rule out “truncated” disks, as those produced by the dynamical ejection of stellar embryos predicted, e.g., by Bate et al. (2003). Let us assume, for example, that the disk has an outer radius of 100 AU, and that, once ejected, loses all material outside a radius of about 10 AU. The mass left depends critically on the unknown density profile of the disk, and may range from about 1/3 (if the surface density profile was $\Sigma \propto R^{-1.5}$) to about 1/10 (for $\Sigma \propto R^{-1.0}$) of the original mass. A disk with mass of only $10^{-4} M_{\odot}$ will live about 3×10^5 years, much less than a typical disk of TTSs, and also much less than the age of many BDs with infrared excess in star-forming regions (e.g., Jayawardhana et al. 2003a). However, if the density profile is very peaked, the difference will not be significant, given the large uncertainties and spread of all the parameters involved. Only very accurate model predictions can be verified or falsified by this kind of arguments.

A final point worth mentioning is that the relation of the accretion rate with the mass and age of the central object may shed light on the physical process by which disk matter accretes onto the central star. The simplest suggestion is that the accretion rate may be related to the temperatures in the disk, which in turn are closely coupled to the luminosity of the central object. This may explain both the dependence of \dot{M}_{ac} on M_{\star} and its decrease with time, since objects of all masses, and BDs in particular, fade as they get older. However, it is not clear that the change in temperature is big enough to account for the changes in \dot{M}_{ac} . More subtle effects can be at work, related for example to the level of chromospheric and coronal activity (and hence X-ray fluxes) of the star and resulting disk ionization (see discussion in Muzerolle et al. 2003).

5. Summary and conclusions

We present in this paper new optical and near-infrared spectroscopic observations of a sample of 19 very low mass objects in the regions Chamaeleon I and ρ Oph. Our main aim was to test if accretion rates could be determined from the intensity of the hydrogen recombination lines in the infrared, namely Pa β and Br γ . This possibility is very important when dealing with large numbers of VLMOs in young star-forming regions such as ρ Oph, where high-resolution spectroscopy in the visual is possible for only a handful of objects.

To this purpose, we have obtained high-resolution H α profiles of all the objects in our sample bright enough to be detectable with UVES on VLT. The comparison of the observed profiles with those predicted by magnetospheric accretion models (Muzerolle et al. 2001) shows that five objects are actively accreting, with \dot{M}_{ac} in the range $\sim 10^{-9} - 10^{-11} M_{\odot}/\text{yr}$, while the remaining three in Cha I have narrow and symmetric profiles, and $\dot{M}_{ac} \lesssim 10^{-12} M_{\odot}/\text{yr}$.

Pa β is detected in emission in 7 of the 10 ρ Oph objects, but only in one in Cha I. We show that the correlation between the Pa β luminosity and the accretion luminosity L_{ac} , found by Muzerolle et al. (1998) for TTS in Taurus over a range of masses $\sim 0.3-1 M_{\odot}$, extends to masses about ten times lower. Whereas the relation between $L(\text{Pa}\beta)$ and L_{ac} (eq.(2)) can certainly be improved when more data will be available, it is already reasonably well defined, and can be used to measure L_{ac} , and consequently \dot{M}_{ac} , for large samples of obscured VLMOs. The results are so far less conclusive for Br γ for which we have a detection in only 2 objects, none with measured accretion rate.

Using eq.(2) and the measured $L(\text{Pa}\beta)$, we determined \dot{M}_{ac} for all the VLMOs in our sample, increasing the number of VLMOs with known \dot{M}_{ac} by more than a factor of two. When plotted as a function of the mass of the central object together with all the existing data on VLMOs and TTS from the literature, our results confirm the trend of lower \dot{M}_{ac} for lower M_{\star} , although with a large spread. Some of the spread is likely due to an “age” effect, namely that, for a given value of M_{\star} , \dot{M}_{ac} decreases strongly with time. Our very young VLMOs in ρ Oph have on average \dot{M}_{ac} at least one order of magnitude higher than objects in older star forming regions. The dependence of \dot{M}_{ac} on central mass and time needs to be better constrained by future observations. However, it is already clear that these data can provide very valuable information on the accretion mechanism in disks during the pre-main-sequence evolutionary phase.

One side product of our analysis is that the width of H α measured at 10% peak intensity correlates quantitatively with \dot{M}_{ac} over a large range of \dot{M}_{ac} and M_{\star} . This supports the currently used criterion to separate accretors from non-accretors among VLMOs according to the H α 10% width (White and Basri 2003) and confirms that a value of 200 km/s (as suggested by Jayawardhana et

al. 2003b) is a rather good threshold value. Furthermore, it suggests that one can use the H α 10% width to obtain a quantitative estimate of \dot{M}_{ac} over a large range of masses. Although the spread of the correlation (eq.(1)) is large, and there are a number of caveats to keep in mind, the possibility of estimating \dot{M}_{ac} without going through rather time consuming model fits is interesting, and deserves further attention.

Finally, we would like to note that high-resolution near-infrared spectroscopy on 8-m class telescopes is becoming available. As with H α for visible objects, high quality infrared line profiles can be compared to model predictions to derive accretion rates for obscured ones. The additional advantage of the IR lines is that they are likely less contaminated than H α by wind/jet emission, flares and stellar activity in general; a sufficiently large sample of objects with measured H α and Pa β profiles will be very valuable in providing more “calibration” points for the line intensity–accretion rate relations, and in better constraining magnetospheric accretion models.

Acknowledgements. This work was partly supported by the MIUR-cofin grant “Low-mass stars and brown dwarfs: formation mechanisms, mass distribution and activity”. We thank the referee (S. Mohanty) for comments that have greatly improved our paper.

References

- Bacciotti F., Ray T.P., Mundt R., Eisloffel J., Solf J. 2002, A&A 576, 222
- Baraffe I., Chabrier G., Allard F., Hauschildt P.H. 1998, A&A 337, 403
- Barrado y Navascués D., Mohanty S., Jayawardhana R., 2004, ApJ, in press
- Bate R.M., Bonnell I.A., Bromm V. 2003, MNRAS 339, 577
- Bontemps S., André Ph., Kaas A.A., et al. 2001, A&A 372, 173
- Calvet N., Hartmann L., Strom S.E. 2000, in “Protostars and Planets IV”, eds Mannings, V., Boss, A.P., Russell, S.S., (Tucson: University of Arizona Press) p. 377
- Comerón F., Rieke G.H., Claes P., Torra J., Laureijs R.J. 1998, A&A 335, 522
- Comerón F., Neuhäuser R., Kaas A.A. 2000, A&A 359, 269
- D’Antona F., Mazzitelli I. 1997, Mem.S.A.It. 68, 807
- Edwards S., Hartigan P., Ghandour L., Andrulis C. 1994, AJ 108, 1056
- Fernández M., Comerón F. 2001, A&A 380, 264
- Folha D.F.M., Emerson J.P. 2001, A&A 365, 90
- Greene T.P., Lada C.J. 1997, AJ 114, 2157
- Gómez M., Persi P. 2001, A&A 389, 494
- Gullbring E., Hartmann L., Briceño C., Calvet N. 1998, ApJ 492, 323
- Jayawardhana R., Mohanty S., Basri G. 2002, ApJ 578, L141
- Jayawardhana R., Ardila D.R., Stelzer B., Haisch K.E. 2003a, AJ 126, 1515
- Jayawardhana R., Mohanty S., Basri G. 2003b, ApJ 592, 282
- Jürgens V., Günther E. 2001, A&A 379, L9
- Liu M.C., Najita J., Tokunaga A.T. 2003, ApJ 585, 372
- Luhman K.L., Rieke G.H. 1998, ApJ 525, 440
- Muzerolle J., Hartmann L., Calvet N. 1998, AJ 116, 2965
- Muzerolle J., Hartmann L., Calvet N. 1998, AJ 116, 455

- Muzerolle J., Calvet N., Hartmann L. 1998, ApJ 492, 743
Muzerolle J., Calvet N., Hartmann L. 2001, ApJ 550, 944
Muzerolle J., Calvet N., Briceo C., Hartmann L., Hillenbrand L. 2000, ApJ 535, L47
Muzerolle J., Hillenbrand L., Calvet N., Briceo C., Hartmann L. 2003, ApJ 592, 266
Natta A., Testi L. 2001, A&A 367, L22
Natta A., Testi L., Comerón F., Oliva E., D'Antona F., Baffa C., Comoretto G., Gennari S., 2003, A&A 393, 597.
Persi P., Marenzi A.R., Olofsson G., Kaas A.A., Nordh L. et al. 20023, A&A 357, 219
Rebull L.M., Hillebrand L.A., Strom S.E., Duncan D.K., Patten B.M., Pavlousky C.M., Makidon R., Adams M.T. 2000, AJ 119, 3026
Testi L., Natta A., Oliva E., D'Antona F., Comerón F., Baffa C., Comoretto G., Gennari S. 2002, ApJ 571, L155
Whelan E.T., Ray T.P., Davis C.J. 2004, A&A 417, 247
White R.J., Basri G. 2003, ApJ 582, 1109
White R.J., Ghez A. 2001, ApJ 556, 265
Wilking B.A., Greene T.P., Meyer M.R. 1999, AJ 117, 469
Williams D.M., Comerón F., Rieke G.H., Rieke M.J. 1995, ApJ 454, 144